

A FREWARE 1D EMITTER MODEL FOR SILICON SOLAR CELLS

Keith R. McIntosh¹ and Pietro P. Altermatt²

¹Centre for Sustainable Energy Systems, Australian National University, Canberra, ACT 0200, AUSTRALIA

²Leibniz University of Hannover, Inst. of Solid-State Physics, Dep. Solar Energy, Appelstrasse 2, 30167, GERMANY

ABSTRACT

Heavily doped surfaces—often called emitters, diffusions, or back-surface fields—are complicated regions of a solar cell. In these regions, the dopant concentration varies over many orders of magnitude in a short distance, causing large variations in the minority carrier concentration, Auger recombination, Shockley–Read–Hall recombination, carrier mobility and even the band gap. Moreover, when the diffusion is heavily doped, the semiconductor becomes degenerate and the carrier concentrations must be calculated with Fermi–Dirac statistics rather than the simpler Boltzmann statistics. Until now, computer simulation packages that account for all of these aspects are either expensive or not freely accessible, and they do not cater specifically to the PV industry. We therefore present a new freeware computer program that models a 1D emitter in silicon. Given a user-defined dopant profile, a surface recombination velocity, and an incident spectrum, the program calculates recombination as a function of depth within the emitter and as a function of the applied voltage. This permits the computation of the emitter saturation current density, the transparency factor, the collection current density, and the collection efficiency. The program can be applied to both phosphorus and boron diffusions and will assist in their optimisation for practical solar cells. In this paper, we present the equations, the assumptions, and the procedure that are employed by the freeware program.

INTRODUCTION

All silicon solar cells contain heavily doped regions. Frequently called “emitters” or “diffusions” or “back-surface fields”, the heavily doped regions have a high concentration of majority carriers and therefore a low concentration of minority carriers. Depending on these concentrations—and on boundary conditions such as the surface recombination velocity and the junction voltage—the presence of a heavily doped region can either increase or decrease the amount of recombination that would otherwise occur. It is critical, therefore, that the dopant concentrations be optimised.

Emitters are often optimised experimentally because they are difficult to model. In an emitter, the dopant concentration varies over many orders of magnitude in a short distance, which causes rapid variation in the minority carrier concentration, Auger recombination, Shockley–Read–Hall (SRH) recombination, carrier mobility and even the band gap. Moreover, when the diffusion is heavily doped, the semiconductor becomes degenerate, and the

carrier concentrations must be calculated with Fermi–Dirac statistics rather than the simpler Boltzmann statistics.

There are computer packages that solve the complete set of semiconductor equations and are capable of accurately modelling emitters [14, 17]; they are, however, expensive and over qualified for the 1D steady-state quasi-neutral solutions that are satisfactory for solar cell studies. The highly useful PC1D freeware program [2] employs neither Fermi–Dirac statistics nor the most recent mobility model and is consequently inaccurate for heavily doped emitters. There are also a plethora of analytical equations that can be used to model emitters that have varying degrees of inaccuracy depending on their level of complexity—well summarised in [6], [10], and [16]—but with modern computer power these analytical solutions save little time compared to the complete numerical solution employed in [6], [18] and this work. Nevertheless, we do not neglect the benefits that understanding such analytical models brings.

The program presented here is the first readily accessible and free computer program that accurately models a heavily doped emitter. We first list the major inputs and outputs of the model, and then summarise the program’s general procedure using an example. The steps are listed and the required equations and assumptions are provided or cited. The program can be attained by contacting either author.

MAJOR INPUTS AND OUTPUTS

The program requires the user to define the following main inputs:

- (i) donor and acceptor dopant profiles,
- (ii) surface recombination velocity,
- (iii) models for mobility and Auger recombination,
- (iv) generation profile (or alternatively, an incident spectrum and transmission curve).

The program then computes the following outputs:

- (i) emitter saturation current J_{0E} ,
- (ii) transparency factor α_T ,
- (iii) collection current J_{LE} ,
- (iv) collection efficiency η_E ,
- (v) a breakdown of the recombination mechanisms.

EXAMPLE AND SUMMARY OF PROCEDURE

The user first defines the donor and acceptor dopant profiles, $N_D(x)$ and $N_A(x)$. Figure 1(a) gives example profiles, where $N_D(x)$ is a Gaussian profile with a surface

concentration of 10^{20} cm^{-3} and a junction depth of $1.5 \mu\text{m}$. This equates to an equilibrium sheet resistance of $10.6 \Omega/\text{sq}$ for a phosphorus-doped diffusion in which 100% of

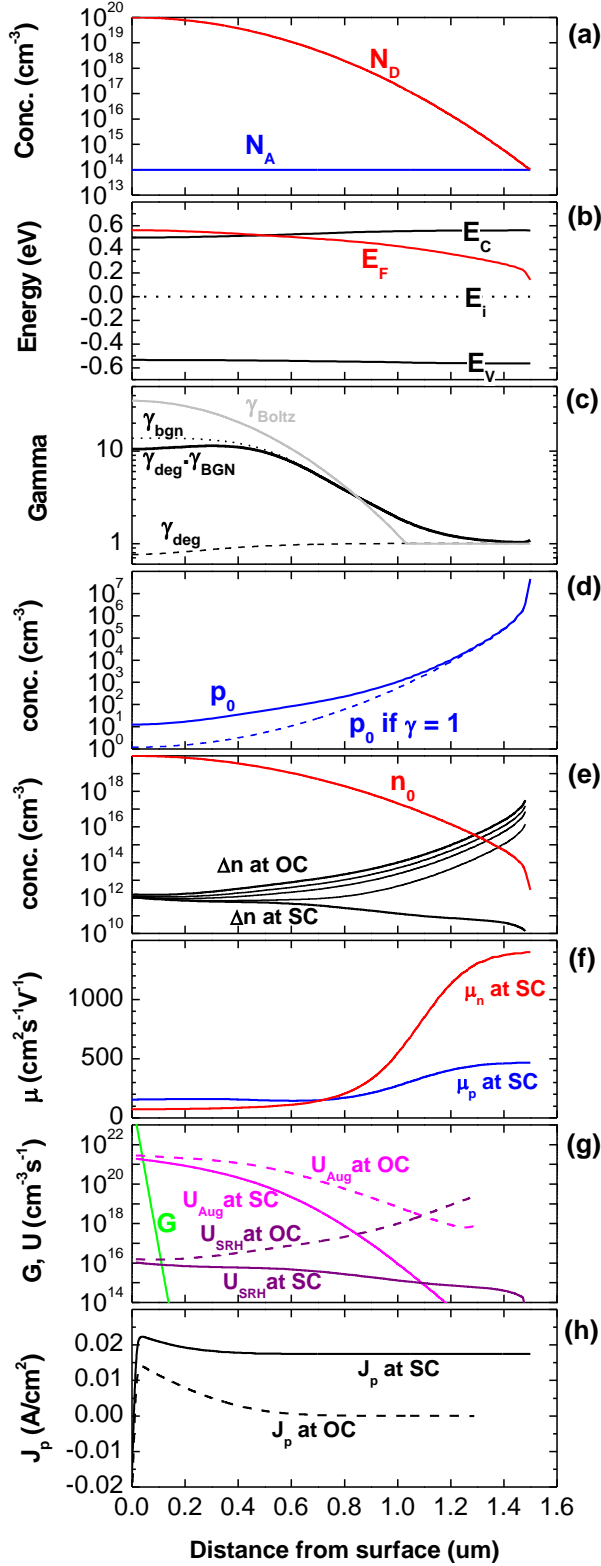


Figure 1: Example simulation as described in the text.

the dopants are activated. In the example, $N_A(x)$ is constant and equal to 10^{14} cm^{-3} , equivalent to a bulk resistivity of $133 \Omega\text{-cm}$ for boron-doped silicon.

With these profiles, the program computes the energy of the conduction band E_c , valence band E_v and Fermi level E_f , all relative to the intrinsic Fermi energy E_i . At first, they are computed at equilibrium—i.e., in the dark with no applied voltage. Figure 1(b) plots this data for the example, showing how the band gap decreases as N_D increases. It also shows how E_f exceeds E_c when N_D is high, meaning that the semiconductor is degenerate and Fermi–Dirac statistics must be employed rather than Boltzmann statistics. Thus, an accurate assessment of this emitter must compute E_c , E_v and E_f with appropriate models for band-gap narrowing (BGN) and degeneracy.

The next step is to determine the product of the electron and hole concentrations, $n(x)p(x)$. In intrinsic silicon, it is equal to the square of the intrinsic carrier concentration n_i^2 , but any change in E_c , E_v and E_f causes it to vary. Instead, $n(x)p(x) = \gamma_{\text{BGN}}\gamma_{\text{deg}}n_i^2$, where γ_{BGN} and γ_{deg} are factors that account for BGN and degeneracy [1]. They are plotted in Figure 1(c). Notice that BGN acts to increase $n(x)p(x)$ while degeneracy acts to decrease $n(x)p(x)$. Combined, $n(x)p(x)$ is greater than n_i^2 , peaking at $N_D \sim 10^{19} \text{ cm}^{-3}$. The figure also plots γ_{Boltz} , which is the single factor that is used to calculate $n(x)p(x)$ when using Boltzmann statistics and a common BGN model [2]; it differs from the more correct prefactor, $\gamma_{\text{BGN}}\gamma_{\text{deg}}$.

Once γ_{BGN} and γ_{deg} have been computed, the program can determine the equilibrium minority carrier concentration. Figure 1(d) compares the hole concentration $p_0(x)$ when it is correctly calculated (solid line) to when it is calculated assuming no BGN or degeneracy. They differ by about an order of magnitude.

With the equilibrium conditions established, the program solves for several steady-state conditions. These include short-circuit (SC) and open-circuit (OC) under illumination, and a range of voltages in the dark. The solutions provide $n(x)$ and $p(x)$ for each steady-state condition, and they require the user to define the generation profile $G(x)$, the surface recombination velocity S , the SRH lifetime in the diffusion τ_D , and models for the carrier mobility and Auger recombination. In this example, $G(x)$ equates to a generation current of $J_G = 40 \text{ mA/cm}^2$, where the wavelength of the incident light is set at 400 nm so that all generation occurs near the front surface (to keep the example simple); S is set at 10^5 cm/s , which is typical of hydrogenated oxide passivation on such heavily doped silicon [1]; τ_D is set at $100 \mu\text{s}$; the mobility model is that of Klaassen [3, 4]; and the Auger model is that of Kerr and Cuevas [5]. The solutions are made using the shooting method and following del Alamo and Swanson’s approach [6, 19] summarised in Appendix C.

Table I: Breakdown of generated current in mA/cm^2 .

	SC	OC
Collected	17.51 (43.8%)	–
Auger recomb in diffusion	6.07 (15.2%)	15.71 (39.3%)
SRH recomb in diffusion	0.00 (0.0%)	0.04 (0.1%)
SRH recomb at surface	16.42 (41.0%)	24.25 (60.7%)
Total	40.00	40.00

Figure 1(e) plots the excess carrier concentration $\Delta n(x)$ (assuming quasi-neutrality, $\Delta n = \Delta p$) for a range of voltages under illumination. Notice how $\Delta n(x)$ increases as the voltage increases from SC to OC. This causes the emitter depth to decrease, as evidenced by the intersection between $\Delta n(x)$ and $n_0(x)$. (Here the emitter is defined by the carrier concentrations rather than the dopant concentrations.) This ‘shrinking’ of the emitter at high voltages is an important aspect that, to our knowledge, has not been considered in other emitter modelling studies that extract a J_{LE} .

Figure 1(f) plots the mobility of holes μ_p and electrons μ_n at SC as determined by the model of Klaassen [3, 4]. In fact, the mobilities are the same at equilibrium and at OC in the low-injection regions of the emitter.

Figure 1(g) plots $G(x)$, SRH recombination $U_{SRH}(x)$, and Auger recombination $U_{Aug}(x)$ in the emitter at SC and OC. It does not plot SRH recombination at the surface U_s (which is more significant than $U_{SRH}(x)$) because its units are $\text{cm}^{-2}\text{s}^{-1}$ rather than $\text{cm}^{-3}\text{s}^{-1}$. In this example, $U_{Aug}(x)$ is much greater than $U_{SRH}(x)$, which is generally true of heavy emitters but not necessarily of light emitters. Table I lists the fraction of photocurrent that is either collected or recombined at SC and OC.

Figure 1(h) plots the hole current $J_p(x)$ at SC and OC. It shows how the current is negative near the surface, meaning that more holes flow to recombine at the surface than flow towards the junction. At SC, $J_p(x)$ at the junction is the collection current from the emitter J_{LE} . At OC, $J_p(x)$ at the junction must be zero (by definition of OC).

Emitters are frequently defined by one of four figures of merit: (i) the saturation current J_{0E} , (ii) the transparency factor α_T (iii) the collection current J_{LE} , and (iv) the collection efficiency η_E (or quantum efficiency). All three of these parameters are determined by the program. In this example they are constant with the applied voltage V_j and determined to be $J_{0E} = 190 \text{ fA/cm}^2$, $\alpha_T = 44.8\%$, $J_{LE} = 17.5 \text{ mA/cm}^2$, and $\eta_E = 43.8\%$.

We now describe the computational steps in detail. The notation assumed the majority carriers are electrons, while analogous equations can be derived when the majority carriers are holes.

COMPUTATIONAL STEPS

- 1) The intrinsic carrier concentration n_i is calculated from three fundamental parameters of intrinsic silicon: the energy of the band gap E_{g0} , the density of valence-band states N_v , and the density of conduction-band states N_c , by the equation,

$$n_i^2 = N_v N_c \exp(E_{g0}/k_B T), \quad (1)$$

where k_B is the Boltzmann constant and T is the absolute temperature.

E_{g0} is determined from one of the following three T -dependent models, as selected by the user: (i) Eq 23 of Pässler [11], (ii) Eqs 4 and 5 of Bludau *et al.* [12] with an extension by Green [13], or (iii) Eq 125 of the Sentaurus manual [14]. And T -dependent values for N_c and N_v are determined from Green [13] following

either the simple formulae (Eqs 14 and 15 in [13]) or the more complex formulae (Eqs 4, 5, 6, 8, 9 and 13 in [13]), as selected by the user.

- 2) The user defines the donor dopant profile $N_D(x)$ and the acceptor dopant profile $N_A(x)$, from which the net doping is calculated,

$$N(x) = N_D(x) - N_A(x). \quad (2)$$

In the same manner as PC1D [2], the diffusion profile can be calculated from uniform, exponential, Gaussian, or ERFC functions, or it can be defined from experimental data.

- 3) The majority carrier concentration is determined as

$$n_0(x) = N(x), \quad (3)$$

which assumes complete ionisation of the dopants.

- 4) Initial values for the majority and minority carrier profiles are determined as

$$n(x) = n_0(x), \text{ and} \quad (4a)$$

$$p(x) = n_i^2/N(x). \quad (4b)$$

These initial values correspond to the silicon being in equilibrium with no BGN or degeneracy.

- 5) BGN is taken into account by calculating the reduction in energy of the valence band edge $\Delta E_v(x)$ and the conduction band edge $\Delta E_c(x)$ from $p(x)$, $n(x)$, $N_A(x)$ and $N_D(x)$ as described by Schenk [7] and shown in Appendix A. The band gap can then be calculated,

$$E_g(x) = E_{g0} - \Delta E_g(x) = E_{g0} - [\Delta E_c(x) + \Delta E_v(x)]. \quad (5)$$

- 6) A new equilibrium $n_0(x)p_0(x)$ product is determined by following Altermatt *et al.* [1] as described in Appendix B. This accounts for BGN and degeneracy, where the latter requires the Fermi–Dirac function. The equilibrium $n_0(x)p_0(x)$ product corresponds to there being no generation or applied voltage.

- 7) The equilibrium minority carrier concentration $p_0(x)$ is then calculated by maintaining the assumption that $n_0(x) = N(x)$.

At this point, one could iterate through Steps 5–7 to determine more precise values for the equilibrium concentrations, $p_0(x)$ and $n_0(x)$. Additional iterations are, however, rarely required because BGN is mostly affected by the majority and not the minority carrier concentration.

- 8) The user defines the generation profile $G(x)$, the surface recombination velocity S , and the SRH minority carrier lifetime in the diffusion τ_D . (A future version of the program will incorporate the full SRH equation.) The user also selects an Auger recombination model. If desired, $G(x)$ is determined for a user-defined spectrum and reflection. Suitable values of S for oxide-passivated Si can be found in [1].

- 9) The minority carrier current $J_p(x)$ and the excess carrier concentration $\Delta p(x)$ are computed in a similar manner to that presented by del Alamo and Swanson [6, 19] and described in Appendix C. They are determined for:

- (a) dark JV curve by sweeping $\Delta p(0)$ when $G(x) = 0$,

- (b) light JV curve by sweeping $\Delta p(0)$ when $G(x) \neq 0$,
- (c) short-circuit by solving for $J_p(x_j) = 0$, and
- (d) open-circuit by solving for $\Delta p(x_j) = 0$.

Here, x_j is defined as x when $n_0(x) = \Delta p(x)$; as evident in Figure 1(e), x_j decreases with increasing V_j .

Steps 9(a)–9(d) entail calculating solutions for $p(x)$, $n(x)$, $\mu_p(x)$, $U(x)$, $U_{SRH}(x)$, $U_{Aug}(x)$ and U_s ; and solutions for $E_v(x)$, $E_c(x)$, $E_{Fp}(x)$ and $E_{Fn}(x)$ relative to E_i . Note that $E_c(x) - E_{Fn}(x)$ is unaffected by BGN because $n_0(x)$ is assumed constant (i.e. $E_c(x)$ and $E_{Fn}(x)$ decrease by the same $\Delta E_c(x)$).

After Step 9, we have steady-state solutions after a single iteration. If the new $p(x)$ and $n(x)$ alter the degree of BGN compared to the equilibrium condition, then additional iterations are required through Steps 5–7 and 9.

10) Lastly, J_{0E} , α_T , J_{LE} , and η_E are calculated as a function of the applied voltage V_j in the following way:

a) J_{0E} is calculated from dark solutions [6, 19, 10] with

$$J_p(x_j) = -J_{0E} \left[\frac{n(x_j)p(x_j)}{n_0(x_j)p_0(x_j)} - 1 \right], \quad (6a)$$

which in low injection simplifies to

$$J_p(x_j) = -J_{0E} \left[\frac{\Delta p(x_j)}{p_0(x_j)} \right]. \quad (6b)$$

Equation 6b is adequate with our definition of x_j . The program determines J_{0E} in the dark over a range of V_j , and remains constant when the dominant source of recombination in the emitter is proportional to $\Delta p(x)$ for all V_j . These conditions are frequently met in practice although J_{0E} can vary with V_j when surface charge is significant (not permitted in the current version of the program) and when SRH recombination in the emitter is dominant.

b) α_T is calculated from the dark solutions as [6, 15]

$$\alpha_T = \frac{J_p(0)}{J_p(x_j)}. \quad (7)$$

It quantifies the fraction of carriers that recombine at the surface rather than in the diffusion.

c) J_{LE} is calculated from light solutions [6, 19, 10] with

$$J_p(x_j) = J_{LE} - J_{0E} \left[\frac{\Delta p(x_j)}{p_0(x_j)} \right], \quad (8)$$

which is the more general equation to Equation 6b and is valid for low injection. The program determines J_{LE} as a function of V_j by assuming J_{0E} to be independent of V_j . Importantly, J_{LE} decreases with V_j when $G(x)$ is significant at $x > x_j$ because x_j decreases with increasing V_j . (In the example above, $G(x)$ is insignificant at $x > x_j$, and hence J_{LE} is constant with V_j .)

d) η_E is defined as [10]

$$\eta_E = \frac{J_{LE}}{J_G} = \frac{J_{LE}}{q \int_{x=0}^{x_j} G(x) dx}, \quad (8)$$

which tends to be constant with V_j because it accounts for the changes in generation as x_j decreases with V_j .

CONCLUSION

This paper described a new freeware computer program that analyses the recombination and collection associated with a phosphorus or boron emitter. It provided the procedure and the many assumptions and equations entailed. The program will permit a more readily accessible means to optimise emitters, determine surface recombination velocities, and to understand the many complexities of an emitter. The program will be upgraded as suggestions (and corrections) from users are received, and a more rigorous description of its equations and assumptions will be developed (compared to that given here). The intention is to have an engagement with the photovoltaic engineers to ensure it provides a valuable optimisation and educational tool. We caution the user, however, that the results of this program—and other programs that solve the semiconductor equations—depend critically on the models employed for the minority carrier mobility, Auger recombination and $\gamma_{bgn} \gamma_{deg} n_i^2$. Problems associated with experimentally determining these models are well described by del Alamo [19].

REFERENCES

- [1] P. P. Altermatt *et al.*, *J. Appl. Phys.* **92**, 3187 (2002).
- [2] P. A. Basore and D. A. Clugston, *Proc. 25th IEEE PVSC*, Washington DC, pp. 211–214 (1996).
- [3] D.B.M. Klaassen, *Solid-State Electronics* **35**, 953, 1992.
- [4] D. B. M. Klaassen, *Solid-State Electronics* **35**, 961, 1992.
- [5] M.J. Kerr, and A. Cuevas, *J. Appl. Phys.* **91**, 2473–2480 (2002).
- [6] J.A. del Alamo, and R.M. Swanson, *IEEE Trans. Electron Dev.* **31**, 1878–1888 (1984).
- [7] A. Schenk, *J. Appl. Phys.* **84**, 3684–3695 (1998).
- [8] R.R. King, R.A. Sinton, and R.M. Swanson, *IEEE Trans. Electron Dev.* **37**, 365–371 (1990).
- [9] R.R. King, and R.M. Swanson, *IEEE Trans. Electron Dev.* **38**, 1399–1409 (1991).
- [10] A. Cuevas, and M. A. Balbuena, *IEEE Trans. Electron Dev.* **36**, 553–560 (1989).
- [11] R. Pässler, *Phys. Rev. B* **6**, 085201 (2002).
- [12] W. Bludau, A. Onton, and W. Heinke, *J. Appl. Phys.* **45**, 1846–1848 (1974).
- [13] M.A. Green, *J. Appl. Phys.* **67**, 2944–2954 (1990).
- [14] SENTAURUS, Synopsys Inc. Mountain View, CA, www.synopsys.com/products/tcad/tcad.html
- [15] J. del Alamo, J. van Meerbergen, F. D’Hoore and J. Nijs, *Solid-State Electronics* **24**, 533–538 (1981).
- [16] A. Cuevas, R. Merchán, and J. C. Ramos, *IEEE Trans. Electron Dev.* **40**, 1181–1183 (1993).
- [17] *ATLAS User’s Manual*, Version 5.12.1.R. Silvaco International: Santa Clara, 2007.

- [18] R.P. Mertens, H.J. De Man, and R.J.V. Overstraeten, *IEEE Trans. Electron Dev.* **20**, 772–778 (1973).
 [19] J. del Alamo, “Minority carrier transport in heavily doped n-type silicon,” Ph.D. dissertation, Stanford University (1985).

APPENDIX A

Here we state the equations from Schenk’s seminal paper on BGN in crystalline silicon [7] that are used in the freeware program. We follow Schenk’s notation where there is no ambiguity, noting that (i) n_e and n_h are the dimensionless electron and hole concentrations that relate to n and p by the excitonic Bohr radius a_{ex} by $n_e \equiv na_{ex}^3$ and $n_h \equiv pa_{ex}^3$; (ii) p_e and p_h are constants and not hole concentrations; (iii) ζ is employed to represent the curly T in [7], which is not available in our equation editor; and (iv) n_{ionic} is used rather than Schenk’s n_i to avoid confusion with the intrinsic carrier concentration defined above.

In [7], Schenk derives equations for BGN from quantum mechanical principles. There are two components that sum to give the total BGN,

$$\Delta E_c = \Delta E_c^{xc} + \Delta E_c^i, \text{ and} \quad (\text{A1a})$$

$$\Delta E_v = \Delta E_v^{xc} + \Delta E_v^i, \quad (\text{A1b})$$

where ΔE_c^{xc} and ΔE_v^{xc} are the rigid quasi-particle shifts of the conduction and valence band edges, which depend on the free-carrier concentrations; and ΔE_c^i and ΔE_v^i are the ionic quasi-particle shifts of the conduction and valence band edges, which depend on the ionised dopant concentrations. Neither are simple to derive or understand. Here, we simply state the relevant equations, in [7],

The rigid quasi-particle shifts are given by

$$\Delta E_c^{xc} = -Ry_{ex}\Delta_e^{xc}, \quad (\text{A2a})$$

$$\Delta E_v^{xc} = -Ry_{ex}\Delta_h^{xc}, \quad (\text{A2b})$$

where (Eq. 33 in [7])

$$\begin{aligned} \Delta_a^{xc} = & - \left\{ (4\pi)^3 n_{\Sigma}^2 \left[\left(\frac{48n_a}{\pi g_a} \right)^{1/3} + c_a \ln(1 + d_a n_p^{p_a}) \right] \right. \\ & \left. + \left(\frac{8\pi\alpha_a}{g_a} \right) n_a \zeta^2 + \sqrt{8\pi n_{\Sigma}} \zeta^{5/2} \right\} \\ & \times \left\{ (4\pi)^3 n_{\Sigma}^2 + \zeta^3 + b_a \sqrt{n_{\Sigma}} \zeta^2 + 40n_{\Sigma}^{3/2} \zeta \right\}^{-1} \end{aligned} \quad (\text{A3})$$

and the ionic quasi-particle shifts are given by

$$\Delta E_c^i = -Ry_{ex}\Delta_e^i, \text{ and} \quad (\text{A4a})$$

$$\Delta E_v^i = -Ry_{ex}\Delta_h^i, \quad (\text{A4a})$$

where (Eq. 37 in [7])

$$\begin{aligned} \Delta_a^i = & -n_{ionic}(1 + U^i) \times \left\{ \sqrt{\zeta n_{\Sigma} / 2\pi} [1 + h_a \ln(1 + \sqrt{n_{\Sigma} / \zeta})] \right. \\ & \left. + j_a U^i n_p^{3/4} (1 + k_a n_p^{q_a}) \right\}^{-1}. \end{aligned} \quad (\text{A5})$$

In Eqs A1 and A1, the subscript, a , represents either h or e . The other parameters are given by $n_{\Sigma} \equiv n_e + n_h$, $n_p \equiv \alpha_e n_e + \alpha_h n_h$, $\zeta \equiv (k_B T / q) / Ry_{ex}$, (these from p. 3689 of [7]), $U^i = n_{\Sigma}^2 / \zeta^3$ (Eq. 38 of [7]), $n_{ionic} = N_{\Sigma} a_{ex}^3$ (p. 3687 [7]), $N_{\Sigma} = N_D + N_A$, $\alpha_a = \mu^* / m_a$, and the remaining variables are listed in Tables I, II and III of [7].

APPENDIX B

Altermatt *et al.* show that Fermi–Dirac rather than Boltzmann statistics must be applied when modelling heavily doped emitters [1]. With Fermi–Dirac statistics, the carrier concentrations relate to the Fermi energies by the equations,

$$\frac{n}{N_c} = F_{1/2} \left[-\frac{E_c - E_{fn}}{k_B T} \right], \text{ and} \quad (\text{B1a})$$

$$\frac{p}{N_v} = F_{1/2} \left[-\frac{E_{fp} - E_v}{k_B T} \right], \quad (\text{B1b})$$

where E_{fn} and E_{fp} are the electron and hole Fermi energies, and $F_{1/2}$ is the Fermi operator of order 1/2, defined as

$$F_j(x) = \frac{1}{\Gamma(j+1)} \int_0^{\infty} \frac{t^j}{\exp(t-x)+1} dt, \quad (\text{B2})$$

$$\Gamma(z) = \int_0^{\infty} t^{z-1} e^{-t} dt, \quad (\text{B3})$$

where

$$\Gamma(3/2) = \sqrt{\pi} / 2. \quad (\text{B4})$$

With the better known Boltzmann statistics, the equations are the same as Equations B1 and B2 except that the $F_{1/2}$ operator is replaced by the exponential operator.

Figure B1 shows how the Fermi–Dirac and Boltzmann equations differ for n/N_c at 300 K. They yield the same result when $E_c - E_{fn} > 0.05$ eV, but diverge as E_{fn} approaches and exceeds E_c ; the latter occurs in samples that are either in very high injection or that are heavily doped, when the semiconductor is said to be degenerate.

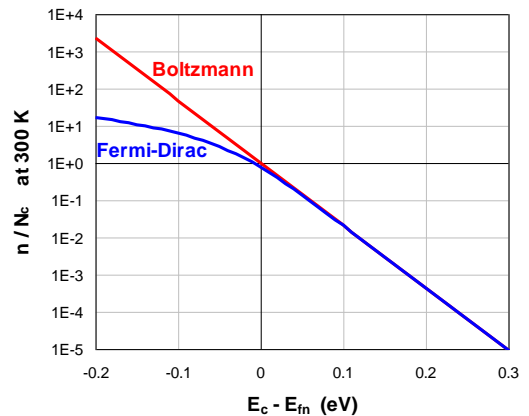


Figure B1: n/N_c calculated by Boltzmann and Fermi–Dirac statistics at 300 K.

Thus, in heavily doped n-type, the pn product can be accurately expressed as

$$pn = N_v \exp\left[-\frac{E_{fp} - (E_{v0} - \Delta E_v)}{k_B T}\right] \times N_c F_{1/2}\left[-\frac{(E_{c0} - \Delta E_c) - E_{fn}}{k_B T}\right], \quad (\text{B5})$$

where p is well approximated with Boltzmann's statistics whereas n must be expressed with Fermi-Dirac statistics.

In [1] it is shown how Equation B5 can be simplified to

$$pn = n_i^2 \times \gamma_{\text{deg}} \times \gamma_{\text{BGN}} \times \exp\left[-\frac{E_{fp} - E_{fn}}{k_B T}\right]. \quad (\text{B6})$$

The degeneracy factor γ_{deg} is dependent on the difference between the intrinsic conduction-band energy E_{c0} and the electron Fermi energy and defined as

$$\gamma_{\text{deg}} = F_{1/2}\left[-\frac{E_{c0} - E_{fn}}{k_B T}\right] / \exp\left[-\frac{E_{c0} - E_{fn}}{k_B T}\right]; \quad (\text{B7})$$

hence, γ_{deg} is the ratio of the functions in Figure B1 and less than unity in heavily doped silicon, approaching unity as doping decreases—evident in Figure 1.

The bandgap narrowing factor γ_{BGN} includes all terms with ΔE_c and ΔE_v and is defined as

$$\gamma_{\text{BGN}} = \exp\left[\frac{\Delta E_v}{k_B T}\right] \frac{F_{1/2}\left[-\frac{(E_{c0} - \Delta E_c) - E_{fn}}{k_B T}\right]}{F_{1/2}\left[-\frac{E_{c0} - E_{fn}}{k_B T}\right]}; \quad (\text{B8})$$

γ_{BGN} increases with doping as evident in Figure 1.

We can now state how the pn product is determined in Step 6 of the computational procedure for n-type silicon:

(6a) Equation B1a is employed to determine

$$F_{1/2}\left[-\frac{E_{c0} - \Delta E_c - E_{fn}}{k_B T}\right], \text{ noting that } E_c = E_{c0} - \Delta E_c$$

and that $n = N_D$.

(6b) The inverse $F_{1/2}$ function is applied to determine

$$\left[-\frac{E_{c0} - \Delta E_c - E_{fn}}{k_B T}\right].$$

(6c) ΔE_c from Step 5 is added to determine

$$\left[-\frac{E_{c0} - E_{fn}}{k_B T}\right].$$

(6d) The pn product is calculated from Equations B6, B7 and B8 using the results of Steps 6a, 6b and 6c. Note that in equilibrium, $E_{Fn} = E_{Fp} = E_F$.

In this appendix, we have stated the relevant equations for heavily doped n-type silicon. Equivalent equations can be derived for heavily doped p-type.

APPENDIX C

We employ the method of Del Alamo and Swanson to solve for $J_p(x)$ and $\Delta p(x)$ [6, 19] though without recourse to

the special solutions. This is only valid in regions of quasi-neutrality, $\Delta p(x) = \Delta n(x)$, and therefore not in depletion regions associated with the junction or with surface charge (or in regions with significant trapping). The solutions are also only valid in regions of low injection, which can be an important stipulation in the lower doped regions deep in the diffusion—as in the example.

This elegant approach combines the effect of drift and diffusion and takes into account the changes in doping and bandgap by solving for $\Delta p(x)/\rho_0(x)$ and $J_p(x)$, where the carrier concentrations are

$$p(x) = \rho_0(x) + \Delta p(x), \quad (\text{C1a})$$

$$n(x) = n_0(x) + \Delta n(x) = N_D(x) + \Delta p(x), \quad (\text{C1b})$$

the minority carrier current equation is

$$J_p(x) = -qD_p(x)\rho_0(x) \frac{d}{dx} \left[\frac{\Delta p(x)}{\rho_0(x)} \right], \quad (\text{C2})$$

the minority carrier continuity equation is

$$\frac{dJ_p(x)}{dx} = q[G(x) - U(x)], \quad (\text{C3})$$

$D_p(x)$ is the diffusivity and equal to $q\mu_p(x)/kT$, and $U(x)$ is calculated from standard models for SRH and Auger recombination, which depend on $p(x)$, $\rho_0(x)$, $n(x)$ and $n_0(x)$.

The two boundary conditions are:

$$J_p(0) = -qS\rho_0(0) \left[\frac{\Delta p(0)}{\rho_0(0)} \right], \quad (\text{C4})$$

and

$$V_j(x_j) = \frac{kT}{q} \ln \left[\frac{\Delta p(x_j)}{\rho_0(x_j)} \right], \quad (\text{C5})$$

where we define x_j as being x when $n_0(x) = \Delta n(x)$, which ensures we do not solve in regions of high injection.

Thus, there are two field equations, two boundary conditions, and two variables, $\Delta p(x)/\rho_0(x)$ and $J_p(x)$. The program solves for these variables using the shooting method with 100 evenly spaced nodes, taking into account the complicated dependencies associated with $\mu_p(x)$ [3, 4], $U(x)$ [5], and x_j on $\Delta p(x)$. It is due to these dependencies—and to the speed of modern computers—that we simply solve the equations numerically and disregard the many analytical approximations [10, 16] or the manipulation [6, 19] used by others.

To our knowledge, it has not previously been recognised that it can be necessary to reduce x_j as V_j increases in order to ensure the solutions correspond to just the low-injection region. As shown in Figure 1e, the emitter enters high injection near the metallurgical junction at high V_j . (In fact, it makes no sense to discuss an emitter in high injection since at this point it is no different to the lower-doped base.) This aspect is critical to an accurate assessment of J_{0E} and J_{LE} at high V_j or when $G(x)$ is significant for $x > x_j$.

By this method one can solve for any $G(x)$, S , and $V_j(x_j)$ (or alternatively $J_p(x_j)$). The program does so for the conditions stated in Step 9.